NANO LETTERS

2008
Vol. 8, No. 4
1219-1223

A ZnO Nanorod Inorganic/Organic Heterostructure Light-Emitting Diode Emitting at 342 nm

X. W. Sun,*,† J. Z. Huang,†,‡ J. X. Wang,† and Z. Xu‡

School of Electrical and Electronic Engineering, Nanyang Technological University, Nanyang Avenue, 639798, Singapore, and Key Laboratory of Luminescence and Optical Information, Ministry of Education, Institute of Optoelectronic Technology, Beijing Jiaotong University, Beijing 100044, People's Republic of China

Received February 4, 2008; Revised Manuscript Received March 6, 2008

ABSTRACT

An inorganic/organic heterostructure light-emitting diode consisting of the hole-transporting layer *N,N′*-di(naphth-2-yl)-*N,N′*-diphenylbenzidine (NPB) and n-type ZnO nanorods fabricated by hydrothermal decomposition is reported. Poly(methyl methacrylate) was used to form a smooth surface on top of ZnO nanorod array with ZnO nanorod tops exposed for subsequent NPB deposition. An unusual ultraviolet emission at 342 nm was observed in the electroluminescence spectrum. Compared to band gap energy of ZnO (3.37 eV), the excitonic emission is blue-shifted and broadened. The mechanism of the blue shift is discussed in terms of the energy band diagram of the heterostructure.

Low-dimensional nanostructural materials have attracted great interest because of their unique physical and chemical properties.[1–4] Among these materials, ZnO, with a direct band gap of 3.37 eV and a large exciton binding energy of 60 meV, has been widely investigated,[5,6] for potential applications in ultraviolet nanolaser sources,[7,8] gas sensors,[9,10] solar cells,[11] and field emission display devices.[12] In the past years, various approaches have been developed to synthesize ZnO nanostructures by means of hydrothermal,[13] metal−organic chemical-vapor deposition,[14] and physical vapor deposition.[15] Recently, the application of ZnO in efficient solid-state lighting is the subject of many studies.[16] However, the light emission from ZnO is mainly based on optical pumping.[17] Although a few electroluminescent devices based on ZnO have been reported,[18–21] an electroluminescent device consisting of an inorganic/organic heterostructure with ZnO nanorods is rare.[22–24]

In this paper, we present a heterostructure lighting-emitting diode made of *N,N′*-di(naphth-2-yl)-*N,N′*-diphenyl-benzidine (NPB) and ZnO nanorods fabricated by aqueous thermal deposition. An excitonic ultraviolet emission at 342 nm was observed in the electroluminescence spectrum of the heterostructure light-emitting diode (LED). The mechanism is discussed.

Experimental Section. Indium tin oxide (ITO) glass substrates (50 Ω/□) used for ZnO nanorod growth were cleaned in an ultrasonic bath with acetone, ethanol, and deionized water. To facilitate the nucleation of ZnO nanorod growth, a film consisting of 50 nm ZnO particles was fabricated on the substrate by ultrasonic spraying pyrolysis. The hydrothermal reaction solution for ZnO nanorod fabrication was prepared by mixing appropriate quantities of ammonia (25%) and zinc acetate, 0.3 M, in 60 mL of deionized water in a bottle with an autoclavable screw cap. The ITO substrate (2 cm × 4 cm) was immersed vertically in the solution, and the sealed bottle was heated to 95 °C for 3 h inside a conventional laboratory oven, and then the bottle was cooled down naturally for 1.5 h before it was taken out. Subsequently, the sample was washed repeatedly with deionized water and dried in air for characterization. Poly(methyl methacrylate) (PMMA) dissolved in toluene with a concentration of 5 mg/mL was spin-coated on the hydrothermally grown product with a rotation rate of 2000 rpm (rotations per minute) to provide a smooth surface for subsequent thin film deposition. Oxygen plasma etching (10 Pa for 15 s) was then applied to remove PMMA coated on top of the ZnO nanorods to expose them for junction formation with NPB. NPB and Ag (80 nm) films were deposited subsequently by thermal evaporation in a high vacuum condition of about 2×10^{-4} Pa. Four devices with different NPB thicknesses of 100 nm (device A), 200 nm (device B), 300 nm (device C), 400 nm (device D) were fabricated for comparison. The schematic diagram of the inorganic/organic heterostructure LED is shown in Figure 1. The morphology was observed using field emission

* Corresponding author, exwsun@ntu.edu.sg.
† Nanyang Technological University.
‡ Beijing Jiaotong University.

10.1021/nl080340z CCC: $40.75
Published on Web 03/19/2008

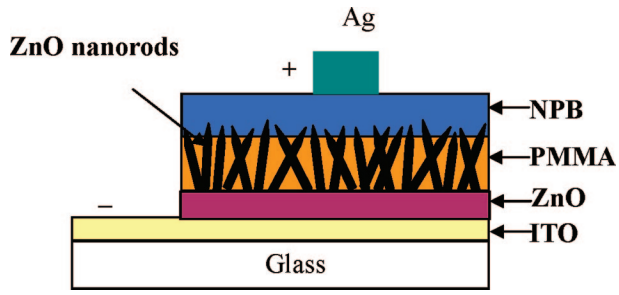

Figure 1. Schematic diagram of the inorganic/organic heterostructure LED.

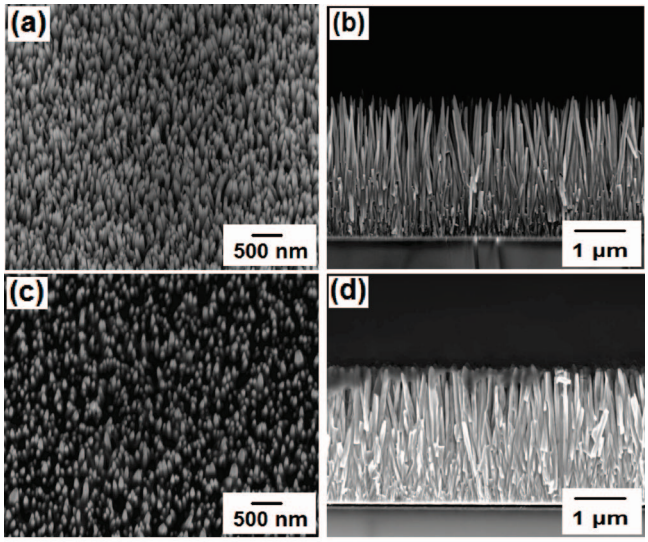

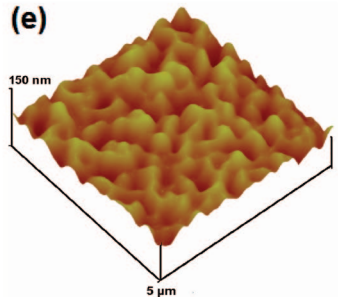

Figure 2. (a) SEM image of the ZnO nanorod array viewed at a 40 ° tilted angle. (b) Cross-sectional SEM image of the ZnO nanorod array. (c) SEM image of ZnO nanorod array embedded in PMMA after plasma treatment viewed at a 40° tilted angle. (d) Cross-sectional SEM image of the ZnO nanorods embedded in PMMA after plasma treatment. (e) Three-dimensional AFM surface image (5 × 5 μm) of ZnO nanorods embedded in PMMA after NPB (200 nm) deposition.

scanning electron microscopy (FE-SEM, JEOL JSM-6340F) and atomic force microscopy (AFM, Nanoscope IIIa Veeco). The current–voltage characteristics were measured by a precision semiconductor parameter analyzer (HP4156A), and the electroluminescence (EL) of the inorganic/organic heterostructure LED was detected by a Si photodiode attached to a spectrometer. The photoluminescence (PL) of ZnO nanorods was excited by a He−Cd laser at 325 nm. The absorption spectrum of NPB is measured with an UV-3101PC spectrophotometer, and the photoluminescence of the NPB is measured with SPEX Fluorolog-3 spectrometer

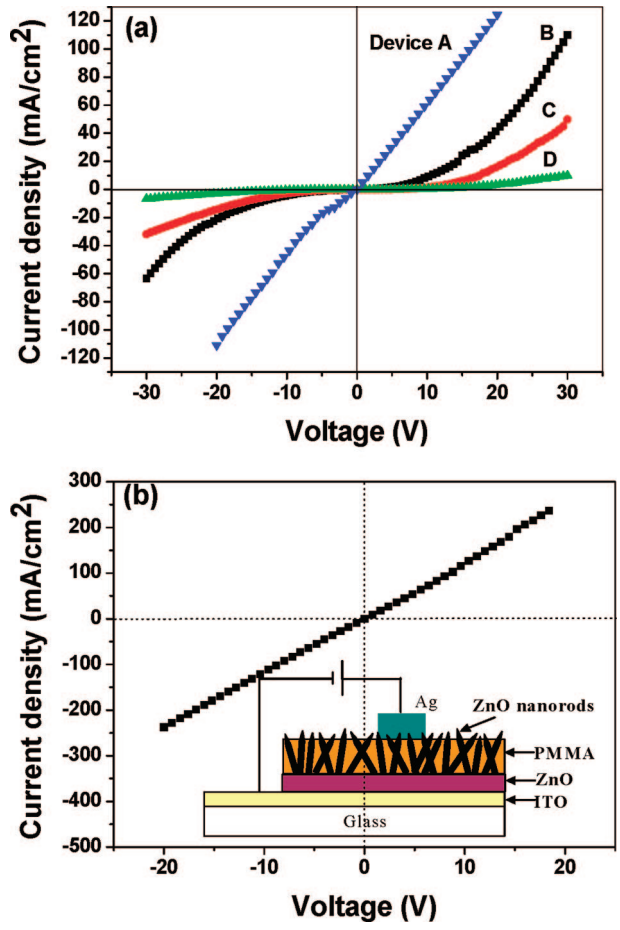

Figure 3. (a) Current–voltage characteristics of the inorganic/organic heterostructure LED devices of A, B, C, and D. (b) Current–voltage characteristics of Ag contact on the ZnO nanorods embedded in PMMA. Inset is the schematic diagram of Ag contact on the ZnO nanorods embedded in PMMA.

(excited at 360 nm). All of these measurements were carried out at room temperature in ambient atmosphere.

Results and Discussion. Panels a and b of Figure 2 show the tilted-view (40°) and cross-sectional SEM images of the as-grown ZnO nanorods, respectively. From panels a and b of Figure 2, we can see that ZnO nanorods are primarily aligned along the perpendicular direction of the substrate with a diameter and height of about of about 150 nm and 2.5 μm, respectively. Panels c and d of Figure 2 show the tilted-view (40°) and cross-sectional SEM image of ZnO nanorods after PMMA coating and oxygen plasma treatment, respectively. The bright spots are the ZnO nanorods, and the dark area is the space between the nanorods solidly filled with PMMA. The function of the PMMA is to form a smooth surface for subsequent NPB deposition. It can be seen from Figure 2d that the PMMA cannot fill up the gaps completely. However, it does serve the function of forming a smoother surface. Figure 2e shows a three-dimensional AFM surface image of the ZnO nanorods embedded in PMMA after NPB (200 nm) deposition. Though the surface is still rough after NPB deposition, with a root mean square roughness of 17.159 nm and a maximum peak−peak roughness of 116 nm, the tips of ZnO nanorods can be covered well by NPB (see the following current–voltage characterization). Good

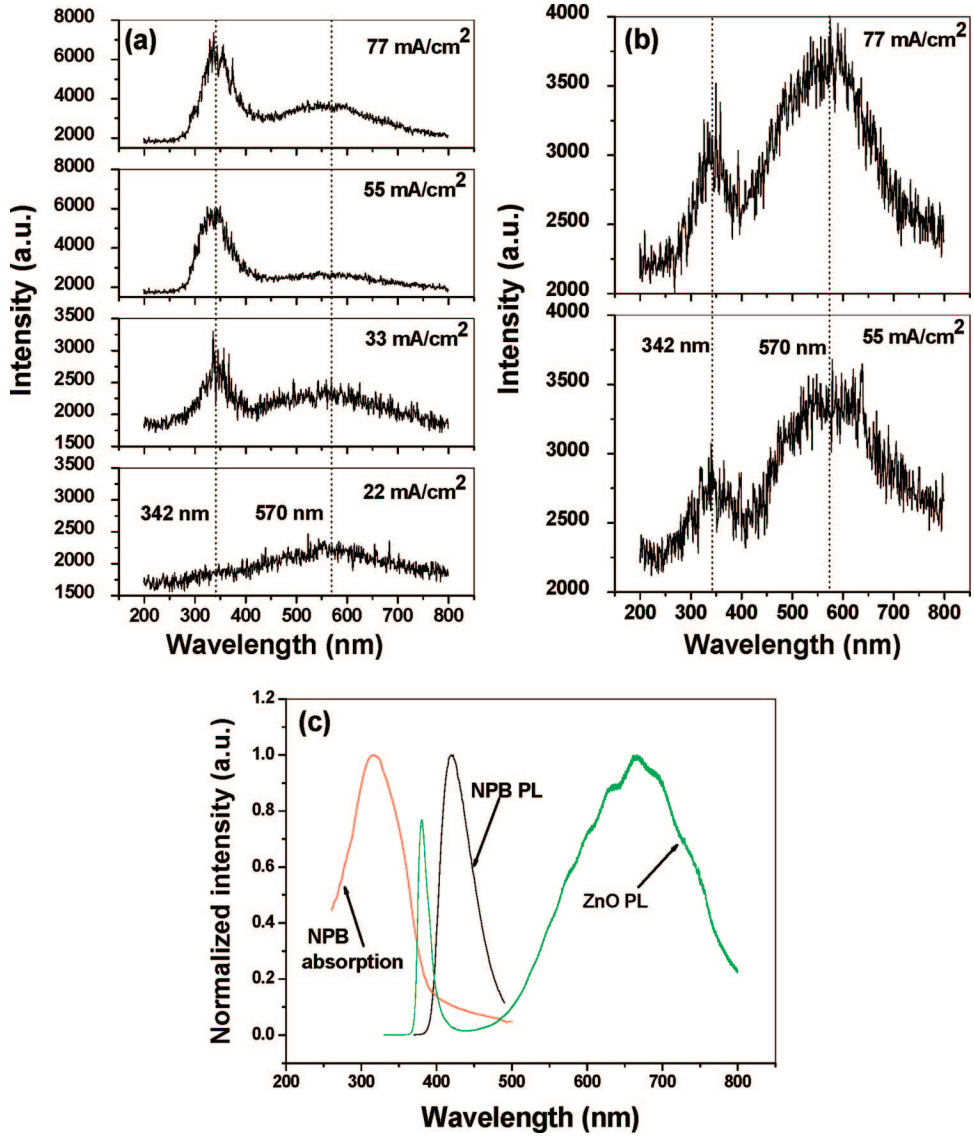

Figure 4. Electroluminescence spectrum of the inorganic/organic heterostructure LED of (a) device B and (b) device C under different current. (c) Photoluminescence spectrum of the ZnO nanorods and absorption and photoluminescence spectrum of NPB.

coverage of NPB is important to facilitate both electron and hole transportation to the heterostructure junction and avoid carrier leakage.

Figure 3a shows the current–voltage characteristics of the inorganic/organic heterostructure LED of devices A, B, C, and D. The current–voltage curves of deivces B, C, and D demonstrate a rectification behavior. The linear current–voltage curve of device A indicates that the NPB layer is too thin to cover ZnO nanorods leading to a direct electron pass from ITO, ZnO nanorods to Ag. Because the NPB layer is too thick in device D, the current is very small compared to devices B and C under the same applied voltage. An Ohmic contact is established between the ZnO nanorods and Ag electrode as indicated in Figure 3b. Thus the rectification diodes behavior shown in Figure 3a comes from the ZnO−NPB heterostructure junction.

The electroluminescence spectra of devices B and C are shown in parts a and b of Figure 4, respectively. A broader defect-related visible emission centered at 570 nm as well as an ultraviolet excitonic emission at 342 nm are observed in both devices B and C. The 342 nm emission is quite broad and extends beyond 300 nm. It is worth mentioning that the electroluminescence spectra of devices B and C are very different from those reported previously in ZnO nanorod inorganic/organic heterostructure devices, where the ultraviolet emissions are located at 383 nm,[22] 390 nm,[23] and 380 nm,[24] respectively. But in the present study, the ultraviolet excitonic emission is centered at 342 nm, which accounts for about a 40 nm blue shift compared to others; besides, the emission peak is broadened. For device B, the 342 nm emission is stronger, but for device C, it is weaker under the same current density (55 and 77 mA/cm^2). Device A does not have electroluminescence as there is no hole current in the device. For device D, the lower current results in no electroluminescence as well. Figure 4c shows the photoluminescence spectrum of ZnO nanorods and the absorption and emission spectra of NPB. The photoluminescence spectrum of ZnO can be clearly identified by the ultraviolet

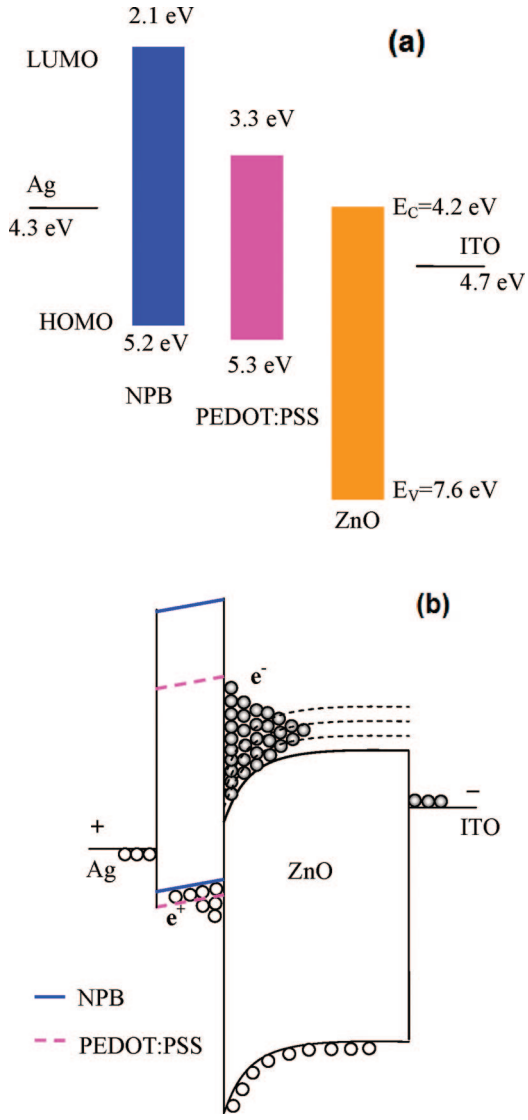

Figure 5. (a) Energy band diagrams of ZnO, NPB, PEDOT/PSS, Ag, and ITO. E_C and E_V represent conduction band and valance band of ZnO, respectively. (b) Energy band diagram of the inorganic/organic heterostructure LED under a positive bias.

emission at 380 nm and defect-related emission at 665 nm. Obviously, the emission spectra in parts a and b of Figure 4 should not be due to the NPB.

The energy band diagrams of all materials used and poly-(3,4-ethylenedioxythiophene)/poly(styrenesulfonate) (PEDOT/PSS) are shown in Figure 5a. Figure 5b shows the band diagram of the inorganic/organic heterostructure LED under positive bias. It can be seen that there is a 0.9 eV barrier for hole injection from Ag to NPB HOMO (highest occupied molecular orbit) and a 2.4 eV barrier for hole injection from NPB HOMO to ZnO valence band. The electron injection barrier is 0.5 eV between the ITO Fermi level and the ZnO conduction band, and there is a 2.1 eV barrier for electron injection from ZnO conduction band to NPB LUMO (lowest unoccupied molecular orbit). So electron and hole accumulation at the ZnO/NPB interface will be substantial under positive bias (Figure 5b).

We propose that the blue shift and broadening (342 nm emission in parts a and b of Figure 4) are related to the electron accumulation at the NPB/ZnO interface (Figure 5b). The accumulation of high concentration electron on the ZnO side results in filling up the conduction band of ZnO (Burstein–Moss effect, also called the band filling effect).[25] Correspondingly, the emission is blue-shifted and broadened.[26,27] Under the low applied voltage (Figure 4a, 22 mA/cm^2), due to a large hole injection barrier (Figure 5a), though there is an electron accumulation at NPB/ZnO interface where the 342 nm emission energy level is formed, there is virtually no hole injection into ZnO valance band, so there is no 342 nm emission. With increased voltage (Figure 4a, 33, 55, and 77 mA/cm^2), holes can be injected into the valance band of ZnO, resulting in 342 nm emission.

In refs 22, 23 and, 24, the hole-transporting layer used was PEDOT/PSS, where the LUMO is much lower (3.3 eV) than that of NPB (2.1 eV) (Figure 5a), so the electron can flow from ZnO to PEDOT/PSS more freely and the accumulation of electron is not significant enough to cause a blue shift. Thus, there is no band-filling effect and no blue shift of ZnO band edge emission observed. The lower intensity of 342 nm emission for device C compared to device B is possibly due to the stronger absorption of a thicker NPB used in device C (Figure 4c).

It is known that ZnO nanorods grown by the solution method present a large number of defects due to the nature of the method, which are reflected by both photoluminescence and electroluminescence (parts c and a of Figure 4, respectively). In refs 23 and 24 with solution grown ZnO nanorods as well but PEDOT/PSS as the hole transporting layer instead of NPB, both the excitonic band edge emission and the visible defect emission in electroluminescence spectrum match well with those in the photoluminescence spectrum; i.e., there is no shift of peaks. However, in our present study, both the band edge and defect emissions are blue shifted in the electroluminescence compared to the photoluminescence. As the blue shift of the band edge emission is due to electron accumulation and the band filling effect of ZnO, we speculate that this is also the cause for the blue shift of the defect emission.

Conclusion. In conclusion, a ZnO nanorod/NPB inorganic/organic heterostructure LED has been reported with broad excitonic ultraviolet emission at 342 nm, which corresponds to the blue-shifted ZnO band edge emission, caused by the ZnO conduction band filling by electron accumulation at the ZnO/NPB interface. The heterostructure ZnO-based LED was fabricated at low temperature, indicating a low-cost process to fabricate UV LEDs. Moreover, such a ZnO-based LED can emit in the UV range which is largely blue shifted from the ZnO band edge emission.

Acknowledgment. X. W. Sun thanks C. M. Lieber of Harvard University for enlightening discussions. Financial support from the Research Grant Manpower Foundation (RGM 21/04) of Nanyang Technological University, Overseas Visiting Research Foundation, and Excellent Doctoral Science and Technology Innovation Foundation of Beijing Jiaotong University (No. 48010) is gratefully acknowledged.

References

(1) Tian, B. Z.; Zheng, X. L.; Kempa, T. J.; Fang, Y.; Yu, N. F.; Yu, G. H.; Huang, J. L.; Lieber, C. M. *Nature* **2007**, *449*, 885–890.

(2) Hayden, O.; Agarwal, R.; Lieber, C. M. *Nat. Mater.* **2006**, *5*, 352–356.

(3) Javey, A.; Nam, S. W.; Friedman, R. S.; Yan, H.; Lieber, C. M. *Nano Lett.* **2007**, *7*, 773–777.

(4) Cui, Y.; Wei, Q. Q.; Park, H. K.; Lieber, C. M. *Science* **2001**, *293*, 1289–1292.

(5) Sun, X. W.; Kwok, H. S. *J. Appl. Phys.* **1999**, *86*, 408–411.

(6) Lee, C. J.; Lee, T. J.; Lyu, S. C.; Zhang, Y.; Ruh, H.; Lee, H. *J. Appl. Phys. Lett.* **2002**, *81*, 3648–3650.

(7) Sun, X. W.; Yu, S. F.; Xu, C. X.; Yue, C.; Chen, B. J.; Li, S. *Jpn. J. Appl. Phys.* **2003**, *42*, L1229–L1231.

(8) Huang, M. H.; Mao, S.; Feick, H.; Yan, H. Q.; Wu, Y. Y.; Kind, H.; Weber, E.; Russo, R.; Yang, P. D. *Science* **2001**, *292*, 1897–1899.

(9) Wang, J. X.; Sun, X. W.; Wei, A.; Lei, Y.; Cai, X. P.; Li, C. M.; Dong, Z. L. *Appl. Phys. Lett.* **2006**, *88*, 233106.

(10) Wang, J. X.; Sun, X. W.; Yang, Y.; Huang, H.; Lee, Y. C.; Tan, O. K.; Vayssieres, L. *Nanotechnology* **2006**, *17*, 4995–4998.

(11) Jiang, C. Y.; Sun, X. W.; Lo, G. B.; Kwong, D. L.; Wang, J. X. *Appl. Phys. Lett.* **2007**, *90*, 263501.

(12) Li, C.; Yang, Y.; Sun, X. W.; Lei; Zhang, X. B.; Wang, B. P.; Wang, J. X.; Tay, B. K.; Ye, J. D.; Lo, G. Q.; Kwong, D. L. *Nanotechnology* **2007**, *18*, 135604.

(13) Wei, A.; Sun, X. W.; Xu, C. X.; Dong, Z. L.; Yang, Y.; Tan, S. T.; Huang, W. *Nanotechnology* **2006**, *17*, 1740–1744.

(14) Tan, S. T.; Chen, B. J.; Sun, X. W.; Fan, W. J.; Kwok, H. S.; Zhang, X. H.; Chua, S. J. *J. Appl. Phys.* **2005**, *98*, 013505.

(15) Kong, Y. C.; Yu, D. P.; Zhang, B.; Fang, W.; Feng, S. Q. *Appl. Phys. Lett.* **2001**, *78*, 407–409.

(16) He, J. H.; Hsu, J. H.; Wang, C. W.; Lin, H. N.; Chen, L. J.; Wang, Z. L. *J. Phys. Chem. B* **2006**, *110*, 50–53.

(17) Baxter, J. B.; Wu, F.; Aydil, E. S. *Appl. Phys. Lett.* **2003**, *83*, 3797–3799.

(18) Ye, J. D.; Gu, S. L.; Zhu, S. M.; Liu, W.; Liu, S. M.; Zhang, R.; Shi, Y.; Zheng, Y. D. *Appl. Phys. Lett.* **2006**, *88*, 182112.

(19) Tsukazaki, A.; Ohtomo, A.; Onuma, T.; Ohtani, M.; Makino, T.; Sumiya, M.; Ohtani, K.; Chichibu, S. F.; Fuke, S.; Segawa, Y.; Ohno, H.; Koinuma, H.; Kawasaki, M. *Nat. Mater.* **2005**, *4*, 42–46.

(20) Lim, J. -H.; Kang, C. -K.; Kim, K. -K.; Park, I. -K.; Hwang, D. -K.; Park, S. -J. *Adv. Mater.* **2006**, *18*, 2720–2724.

(21) Bao, J. M.; Zimmler, M. A.; Capasso, F.; Wang, X. W.; Ren, Z. F. *Nano Lett.* **2006**, *6*, 1719–1722.

(22) Chang, C. -Y.; Tsao, F. -C.; Pan, C. -J.; Chi, G. -C.; Wang, H. -T.; Chen, J. -J.; Ren, F.; Norton, D. P.; Pearton, S. J.; Chen, K. -H.; Chen, L. -C *Appl. Phys. Lett.* **2006**, *88*, 173503.

(23) Könenkamp, R.; Word, R. C.; Godinez, M *Nano Lett* **2005**, *5*, 2005–2008.

(24) Könenkamp, R.; Word, R. C.; Schlegel, C. *Appl. Phys. Lett.* **2004**, *85*, 6004–6006.

(25) Yang, Y. H.; Chen, X. Y.; Feng, Y.; Yang, G. W. *Nano Lett.* **2007**, *7*, 3879–3883.

(26) Lu, J. G.; Fujita, S.; Kawaharamura, T.; Nishinaka, H.; Kamada, Y.; Ohshima, T.; Ye, Z. Z.; Zeng, Y. J.; Zhang, Y. Z.; Zhu, L. P.; He, H. P.; Zhao, B. H. *J. Appl. Phys.* **2007**, *101*, 083705.

(27) Fuchs, F.; Schmitz, J.; Obloh, H.; Ralston, J. D.; Koidl, P. *Appl. Phys. Lett.* **1994**, *64*, 1665–1667.

NL080340Z